mater.scichina.com link.springer.com

Sci China Mater 2025, 68(4): 1212–1219
https://doi.org/10.1007/s40843-024-3236-6

Leaky integrate-and-fire and oscillation neurons based on ZnO diffusive memristors for spiking neural networks

Liang Wang[1,2], Le Zhang[2], Shuaibin Hua[2], Qiuyun Fu[1*] and Xin Guo[2*]

ABSTRACT **Diffusive threshold switching (TS) memristors have emerged as a promising candidate for artificial neurons, effectively replicating neuronal functions and enabling spiking neural networks (SNNs) to emulate the low-power processing of biological brains. In this study, we present an artificial neuron based on a Pt/Ag/ZnO/Pt volatile memristor, which exhibits exceptional TS characteristics, including electroforming-free operation, low voltage requirements (<0.2 V), high stability (2.25% variation over 1024 cycles), a high on/off ratio (10^6), and inherent self-compliance. These Pt/Ag/ZnO/Pt diffusive memristors are employed to simultaneously emulate oscillation neurons and leaky integrate-and-fire (LIF) neurons, enabling precise modulation of oscillation and firing frequencies through pulse parameters while maintaining low energy consumption (1.442 nJ per spike). We further integrate the oscillation and LIF neurons as input and output neurons, respectively, in a two-layer SNN, achieving a high classification accuracy of 89.17% on MNIST-based voltage images. This work underscores the potential of ZnO diffusive memristors in emulating stable artificial neurons and highlights their promise for advanced neuromorphic computing applications using SNNs.**

Keywords: threshold-switching memristor, volatile diffusive memristor, oscillation neurons, leaky integrate-and-fire neurons, spiking neural networks

INTRODUCTION

As human society advances into the era of big data, artificial intelligence (AI), implemented through artificial neural networks (ANNs) based on traditional computer hardware, faces challenges in terms of data processing and energy efficiency [1,2]. The human brain, primarily functioning through spiking neural networks (SNNs) and operating at petaflop speeds while consuming less than 20 watts, demonstrates efficient, real-time, ultralow-power data processing, inspiring the potential of neuromorphic computing to revolutionize technology [3,4]. SNNs support large-scale parallel processing, offering a means to overcome the limitations of the von Neumann architecture. Therefore, breakthroughs in AI will hinge on the development of highly compact artificial neurons and synapses. Conventional complementary metal-oxide semiconductor (CMOS) technology, which relies on intricate auxiliary circuits to emulate biological dynamics, encounters significant challenges in scalability and efficiency for constructing artificial neurons and synapses [5].

Memristors, highly scalable two-terminal devices with low power consumption, have emerged as a promising technology that can function as artificial neurons and synapses, significantly reducing both the complexity and energy consumption of systems. In particular, the realization of spiking neurons, which convert input signals into discrete spikes, is a key to the advancement of artificial neuromorphic systems [6]. Artificial neurons can be effectively emulated using memristors characterized by volatile threshold switching (TS) properties and complex dynamic behaviors [7–10]. Innovations in materials and design have enabled the development of various artificial neuron devices, including metal-insulator transition (MIT) [11–13], ovonic threshold switching (OTS) [14–16], and conductive-bridge random-access memory (CBRAM) [17–19]. Recently, the diffusive TS memristor, a newly developed CBRAM, employs silver (Ag) or copper (Cu) as the active electrode or dopant in solid electrolytes, which has gained great attention [20]. These diffusive TS memristors provide low leakage characteristics, high performance, and excellent integration potential with the CMOS technology [20,21]. Current reports highlight several innovative artificial neurons constructed from simple devices utilizing metal oxides such as SiO_2 [22,23], HfO_2 [24,25], and TaO_x [26–28], with an Ag top electrode. However, most of these diffusive TS devices require electroforming and exhibit restricted on-state currents. When the compliance current (I_{cc}) exceeds 10 μA, volatile TS generally converts into a nonvolatile memory due to stable growth of conductive filaments (CFs) [21]. Meanwhile, the stochastic nature of filament formation, driven by the movement of active metal ions, can result in increased performance variability, thereby impeding the advancement of reliable artificial neurons [29]. Therefore, there is an urgent need to develop artificial neurons based on metal-filament TS memristors that operate without electroforming and current limiting, ensuring consistent and stable performance for practical applications.

Several studies have demonstrated that diffusive TS memristors can effectively function as leaky integrate-and-fire (LIF) neurons [30–33] or oscillation neurons [34,35]. These findings highlight promising potential of diffusive TS memristors for applications in neuromorphic systems. However, there is con-

[1] Engineering Research Center for Functional Ceramics of Ministry of Education, School of Integrated Circuits, Huazhong University of Science and Technology, Wuhan 430074, China
[2] State Key Laboratory of Material Processing and Die & Mould Technology, School of Materials Science and Engineering, Huazhong University of Science and Technology, Wuhan 430074, China
* Corresponding author (email: fuqy@mail.hust.edu.cn; xguo@hust.edu.cn)

siderable randomness in oscillation intervals when the device functions as oscillatory neurons, as well as in integration time when it operates as LIF neurons. Besides, diffusive TS devices that can simultaneously exhibit both oscillation and LIF neurons functionalities have been rarely reported. Therefore, developing novel architectures, which integrate stable oscillation behavior and LIF functions, is essential for advancing neuromorphic technology.

In this work, diffusive memristors based on Pt/Ag/ZnO/Pt demonstrate excellent volatile threshold-switching characteristics, fast turn-on delay time and endurance exceeding 10^5 cycles. These stable TS properties enable the memristors to effectively emulate both LIF and oscillation neurons, which respond well to applied electronic stimuli. As the input pulse width increases, the number of pulses required for firing decreases, indicating a higher output spike frequency. Additionally, the oscillation frequency increases nearly linearly with the input pulse voltage. More importantly, we developed a fully connected SNN using ZnO memristors for MNIST image classification, achieving an accuracy of 89.17% after 50 epochs. This demonstrates the potential of ZnO memristors in constructing efficient and high-performance neuromorphic systems for complex computational tasks.

EXPERIMENTAL SECTION

Device fabrication

Crossbar structured Pt/Ag/ZnO/Pt/Ti memristive devices were fabricated on silicon wafers with a 500 nm thermal oxide layer, utilizing a combination of standard photolithography and magnetron sputtering technologies. Sequentially, a Ti adhesive layer (5 nm) and a Pt bottom electrode (20 nm) were deposited via direct current (DC) sputtering, followed by a ZnO layer (30 nm) using radio frequency (RF) sputtering in an Ar:O_2 (14:1) mixture. An Ag top electrode (10 nm) and Pt (55 nm) were then deposited. The fabricated devices were annealed in ambient air at 300°C for 2 h.

Characterizations and electrical measurements

The microstructure of the Pt/Ag/ZnO/Pt/Ti device was analyzed using an FEI Tecnai G2 F30 transmission electron microscope (TEM) equipped with energy-dispersive X-ray spectroscopy (EDS). Samples for TEM analysis were crafted using a Helios G4 UX focused ion beam. Additionally, atomic force microscopy (AFM) was employed to examine surface topography. To determine the chemical composition of the as-deposited ZnO film, X-ray photoelectron spectroscopy (XPS) was used for material characterization analyses. Electrical measurements were performed using a Keithley 4200 SCS system.

RESULTS AND DISCUSSION

Fig. 1a illustrates the schematic structure of a two-terminal volatile threshold-switching device, featuring a Pt/Ag/ZnO/Pt configuration fabricated on a SiO_2/Si substrate. The device exhibits a classic metal-insulator-metal structure, incorporating a top electrode of Pt-capped Ag, an intermediary ZnO thin film, and a bottom Pt electrode with an adhesive Ti layer. The Pt/Ag/ZnO/Pt memristor is fabricated using a bottom-up deposition approach, integrating magnetron sputtering with photolithography techniques. The device features a crossbar architecture with an active area of 10 μm × 10 μm. Following the fabrication process, the device was subjected to post-annealing at 300°C for 2 h in air. Fig. 1b features a cross-sectional view obtained through TEM, alongside EDS mapping that shows the distribution of Pt, Ag, Zn, and Ti elements. The distinct layered structure is clearly observed, and the inset high-resolution TEM (HRTEM) image indicates that Ag remains unoxidized during annealing process. Additionally, EDS confirms partial diffusion

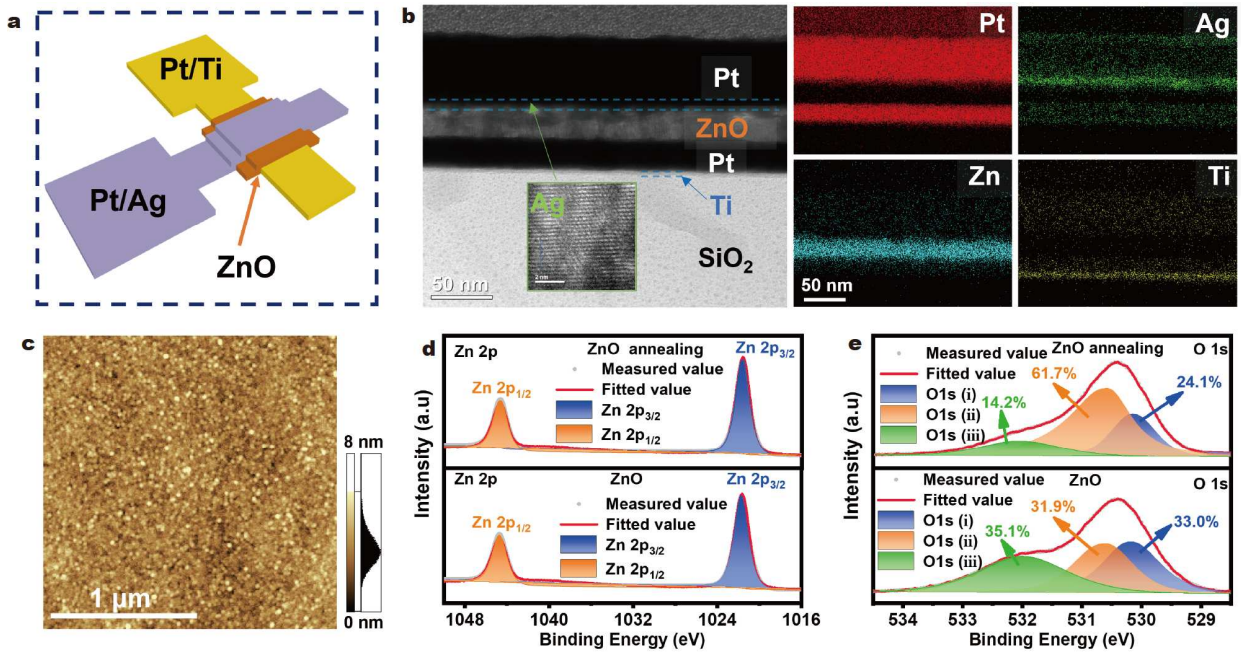

Figure 1 Characterizations of Pt/Ag/ZnO/Pt memristor. (a) Schematic illustration of the Pt/Ag/ZnO/Pt device with a crossbar two-terminal structure. (b) The cross-sectional TEM image alongside EDS mapping of Pt/Ag/ZnO/Pt/Ti device. The inset is an HRTEM image of the Ag film. (c) Surface topography of the ZnO film over a 2 μm × 2 μm area acquired through AFM analysis. The XPS spectra of (d) Zn 2p and (e) O 1s with and without annealing process.

of the Ag layer into the ZnO layer, which contributes to the forming-free behavior of the device and significantly enhances its cycling stability. Fig. 1c depicts the ZnO film's surface topography characterized through AFM, which demonstrates an exceptionally smooth surface with a root-mean-square (RMS) roughness of just 1.104 nm. The above results depict the multilayered structure of the Pt/Ag/ZnO/Pt device, offering a detailed understanding of the structure of the TS artificial neuron.

XPS analyses were employed to analyze the surface composition and chemical state of the ZnO films before and after annealing, with spectra calibrated to the C 1s binding energy (284.8 eV). Fig. 1d illustrates the XPS spectra of the Zn 2p for two samples, both revealing two distinct peaks at 1021.65 and 1044.60 eV. These peaks correspond to Zn $2p_{3/2}$ and Zn $2p_{1/2}$ of the ZnO thin film, confirming that Zn within the ZnO films is in the +2 oxidation state [36–38]. The analyses of oxygen vacancies and interstitial oxygen defects were effectively conducted by examining the chemical state of the O 1s region. As illustrated in Fig. 1e, the XPS spectra of the O 1s in two ZnO samples exhibit an overlay of three distinct peaks. After fitting, these peaks, designated as O (i), O (ii), and O (iii), are positioned at approximately 530.13, 530.57, and 532.01 eV, respectively. The O (i) peak primarily belongs to the lattice oxygen in ZnO [39,40]. Meanwhile, the O (ii) and O (iii) peaks correspond to O^{2-} ions in the oxygen deficient regions and chemisorbed oxygen, respectively [36,41]. The lattice oxygen vacancies facilitate the development of diffusion pathways for Ag^{+} ions [42,43]. It is worth noting that the proportion of the O (ii) peak in the annealed sample (67.1%) is significantly higher than that in the unannealed sample (31.9%). Consequently, the annealed ZnO device exhibits excellent electrical performance, including enhanced stability, faster response speed and even forming-free operation.

The diffusive memristor utilizes electrochemical metallization (ECM) as its switching mechanism, where the application of a bias voltage causes silver ions to migrate and form CFs in areas of high electric field [44,45]. Notably, we investigated the threshold switching characteristics of the Pt/Ag/ZnO/Pt device without employing electrochemical forming process. The typical current-voltage (*I-V*) curve of the Pt/Ag/ZnO/Pt TS device, acquired through alternating voltage sweeps between 0 and 0.3 V in 5 mV steps, is illustrated in Fig. 2a. The device demonstrates remarkable volatile TS behavior, showing no significant degra-

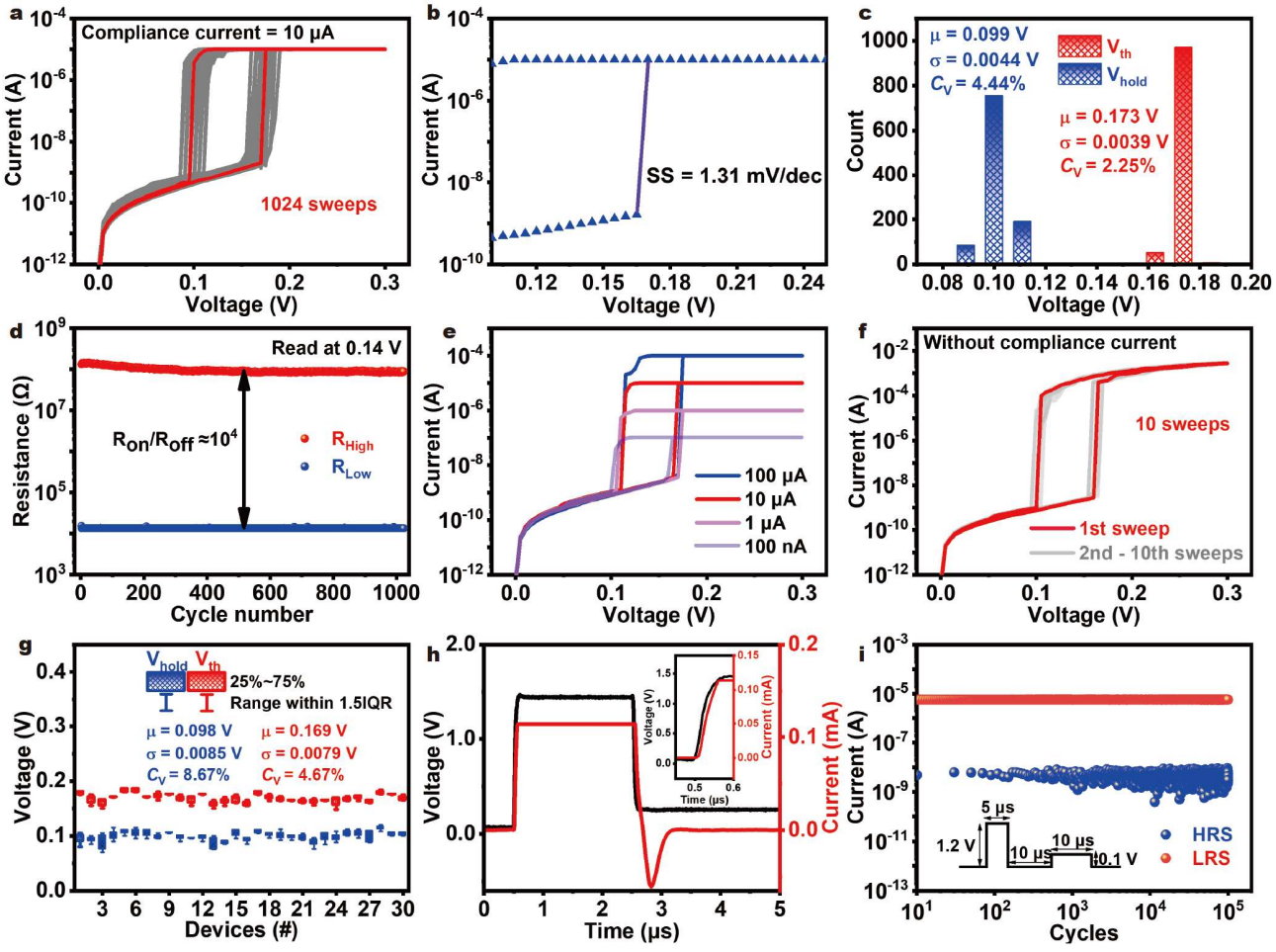

Figure 2 Electrical characterizations of the Pt/Ag/ZnO/Pt device. (a) Current-voltage characteristic curves for 1024 switching sweeps. (b) Switching slope of the device during the initial sweep. (c) The corresponding histogram of V_{th}/V_{hold} and (d) the distributions of LRS/HRS during 1024 switching cycles. *I-V* characteristics of the Pt/Ag/ZnO/Pt device (e) under various compliance currents and (f) without I_{CC}. (g) Distribution of V_{th}/V_{hold} over 10 sweeps from 30 devices. (h) Turn-on speed under a 1.5 V/10 μs pulse and a 0.2 V reading voltage. The inset illustrates its turn-on delay time. (i) 10^5 switching cycles of the device at room temperature.

dation during 1024 consecutive sweeps at an I_{CC} of 10 μA. The device starts in a high resistance state (HRS, OFF) of roughly 130 MΩ at 0.14 V, with a low leakage current of about 2 nA. Upon achieving the threshold voltage (V_{th}) of about 0.17 V, the formation of CFs leads to a swift transition from an HRS to a low resistance state (LRS, ON) with a steep slope (SS) of 1.31 mV dec^{-1} (Fig. 2b). Then, the device reverts to the HRS as the voltage falls below the hold voltage (V_{hold}) of around 0.1 V. The device exhibits excellent cycling stability, with cumulative probability variation (C_v) of 2.25% for V_{th} and 4.44% for V_{hold} (shown in Fig. 2c), alongside a switching ratio of approximately 10^4 (Fig. 2d). Table 1 presents a summary of recently reported artificial neurons utilizing diffusive TS memristors. Our device exhibits lower operating voltage, enhanced stability in threshold voltage variation, and self-limiting current capabilities, which support both LIF and oscillatory neuron functionalities.

Fig. 2e demonstrates the multi-level TS characteristics of the device under various compliance currents from 100 nA to 100 μA. The V_{th} and V_{hold} under different compliance currents are obviously similar, which reveals marked consistency in both V_{th} and V_{hold}. Additionally, the device demonstrates a notably low set power of 16.5 nW, calculated using $P = V_{th} \times I_{th}$, which is lower than those of other TS memristors [32]. Furthermore, it is worth noting that the device still displays volatile TS behavior even at the absence of a limiting I_{CC}, highlighting its self-compliance characteristics and high On/Off ratio of about 10^6, as shown in Fig. 2f.

To evaluate the variation among devices, 30 devices were randomly selected and subjected for 10 DC sweeps, and the distribution of threshold voltages among the various devices is illustrated in Fig. 2g. The average value (μ) and the standard deviation (σ) of V_{th} are 0.169 and 0.0079 V, respectively, with a value of σ/μ at 4.67%, indicating a high level of consistency between devices.

The On-Off switching speed of the Pt/Ag/ZnO/Pt device was evaluated through pulse measurements, as depicted in Fig. 2h. The device can be triggered by applying a voltage pulse of 1.5 V with a duration of 2 μs, and the turn-on delay time is roughly 20 ns. Furthermore, as illustrated in Fig. 2i, the endurance test was conducted using programming pulses, with 1.2 V/5 μs set pulse and 0.1 V/10 μs read pulse, incorporating a 10 μs interval. The device exhibits an endurance exceeding 10^5 cycles, indicating that the device has robust electrical properties across general operating conditions.

In biological neural networks, neurons integrate input signals from presynaptic connections via synapses and generate an action potential upon reaching a specific membrane potential threshold [51,52]. This mechanism has inspired the development of artificial neurons within electronic frameworks intended to emulate SNN functions. Among the primary types of neurons are LIF neurons, which accumulate signals over time and space, and oscillation neurons, which encode inputs into spike trains. Diffusive memristors stand out in mimicking biological neuronal behavior more effectively than other TS memristors, owing to their close resemblance to the ionic drift and diffusion processes in neurons [18,33].

The LIF neurons utilizing diffusive TS memristors facilitate efficient processing of temporal information. When diffusive memristors are exposed to a series of input voltage pulses (V_{in}), silver ions diffuse and form CFs. After applying sufficient pulses, these filaments connect the electrodes, allowing current to flow —a progress called firing. During the resting phase, the silver filament dissolves, returning the device to its initial state, thus emulating the behavior of LIF neurons.

The artificial LIF neuron circuit, which is composed of a Pt/Ag/ZnO/Pt device, a capacitor C (47 nF), and a resistor R (1 MΩ), is illustrated in Fig. 3a. Here, the capacitor functions as the cell membrane by storing charges, while the device acts as an ion channel, generating action pulses. The interval between input signals influences the generation of output action potentials [32]. Fig. 3b–e illustrate the output voltage (V_{out}) corresponding to a sequence of 100 input pulses, each with an amplitude of 2 V, a fixed interval of 200 μs between pulses, and pulse widths of 200, 400, 500, and 600 μs. The capacitor charges when the device is in HRS and discharges upon reaching the threshold voltage (the device is in LRS). The device switches back to HRS once the voltage drops below the V_{hold}, subsequently starting the next charge process. The artificial LIF neuron requires more input pulses to generate the initial action potential, with the first output spike exhibiting the highest voltage under discrete pulse stimulation. This is likely due to the 200 μs interval between pulses, during which Ag ions partially diffuse away from the filament region. As a result, the first spike requires more pulses and a higher voltage to overcome ion diffusion and form a stable filament, leading to a higher voltage compared to subsequent spikes. Obviously, as the input pulse width increases, the number of pulses required for firing decreases, indicating a higher output spike frequency, as shown in Fig. 3f.

In neuromorphic computing, oscillation neurons are fundamental, as they encode input signals into spike strains. Artificial oscillation based on diffusive TS memristors can replicate neural self-oscillation behaviors upon the application of voltage, and parameters such as oscillation frequency can be strategically employed to encode and retain the information from input voltages [53].

Table 1 Comparison with literature reported artificial neurons based on diffusive TS memristors

Device structure	V_{th}/V_{hold} (V)	V_{th} variation	Self-compliance	Neuron type	Energy/spike	Ref.
Ag/TaO_x/ITO	~0.3/0.1	– (1000 cycles)	×	LIF	250 nJ	[26]
Pt/Ag NDs/HfO_2/Pt	0.607/0.201	4.8% (–)	×	Oscillation	–	[35]
Pt/Ag/TiN/$HfAlO_x$/Pt	0.4/~0	6.3% (200 cycles)	×	LIF	16 pJ	[46]
Ag/ZrO_x/Pt	0.4/0.02	5.6% (50 cycles)	×	LIF	–	[47]
Ag/IGZO/ITO	1.69/0.18	12% (50 cycles)	×	LIF	–	[48]
Pt/Ag/SiO_2 NRs/Ag/Pt	0.5/0.3	– (500 cycles)	√	LIF	–	[49]
Au/Ag/hBN/Au/Ti	0.202/0.024	16.8% (500 cycles)	×	LIF	634 pJ	[50]
Pt/Ag/ZnO/Pt	0.17/0.1	2.25% (1000 cycles)	√	LIF & Oscillation	1.442 nJ	This work

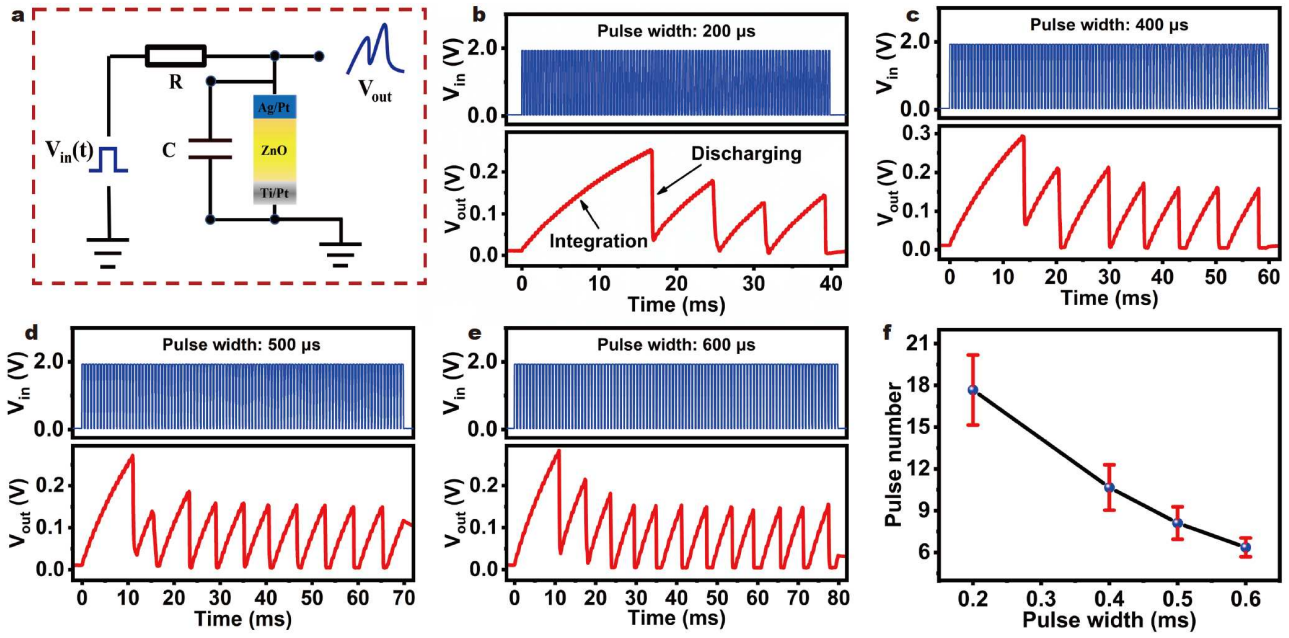

Figure 3 The Pt/Ag/ZnO/Pt LIF neuron circuit and output voltage responses. (a) Schematic of the LIF neuron circuit. (b–e) The output voltages across the device under different pulse width of 200, 400, 500, and 600 μs. (f) Average and standard deviation of pulse number required for firing versus pulse width. The results include the input pulses required for the first spike, and the averages and standard deviations were calculated based on all output spikes.

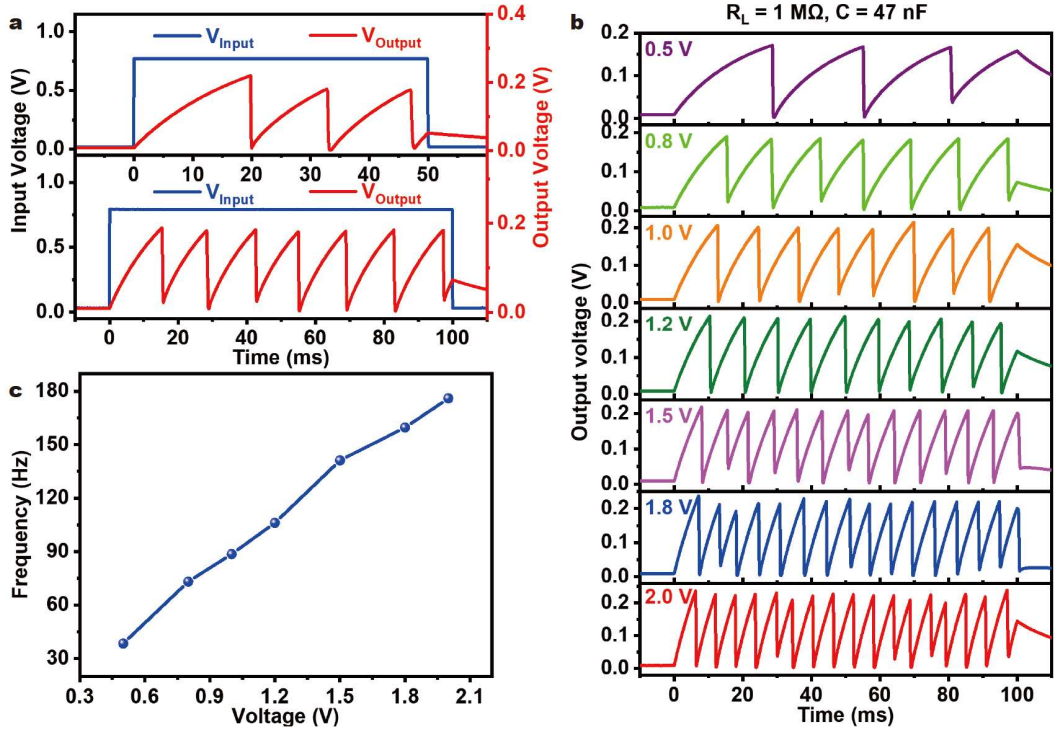

Figure 4 Oscillation characteristics of the Ag/ZnO/Pt neuron device. (a) Self-oscillation at 0.8 V pulse with durations of 50 and 100 ms. (b) The output wave responses to square pulses (100 ms) with different input voltage. (c) Oscillation frequency as a function of input voltage.

For the development of artificial oscillation neurons, a Pt/Ag/ZnO/Pt device was incorporated into a simple RC circuit, which is identical to that of the LIF neuron, as depicted in Fig. 3a. The oscillation neuron circuit includes a parallel capacitance of 47 nF and a series resistor of 1 MΩ. When a suitable input pulse is applied, the capacitor charges and raises the device's potential. Upon reaching the threshold voltage, the device rapidly transitions to the LRS, releasing the capacitor's stored charges and firing an output spike. This causes a decrease in the capacitor's potential, allowing the device to return to the HRS. Consequently, output voltage oscillations occur due to the continuous TS within the Pt/Ag/ZnO/Pt device.

Fig. 4a illustrates the self-oscillation characteristics of the Pt/Ag/ZnO/Pt device under input voltage pulses of 0.8 V with

widths of 50 and 100 ms. In both cases, stable and reversible spikes are sustained until the removal of the applied voltage pulse. Additionally, their oscillation frequencies are nearly identical: 73.1 Hz for 50 ms duration and 73.5 Hz for 100 ms duration. The oscillation frequency is calculated by dividing the total interval time between the first and last pulses by the number of pulse intervals. We investigated the oscillation behavior of the artificial neuron by applying varied input voltage amplitudes, effectively simulating the response of biological neurons to different stimulus intensities, as shown in Fig. 4b. When an input voltage of 0.5 V is applied, the ZnO TS device exhibits stable oscillation behavior, with an average energy consumption of 1.442 nJ per spike, demonstrating its capability as a low-voltage and low-power artificial neuron. Moreover, the artificial neuron exhibits stable oscillatory output spikes across different input voltages ranging from 0.5 to 2 V. The oscillation frequency increases nearly linearly from 38 to 176 Hz as V_{in} increases, as illustrated in Fig. 4c. The voltage-controlled self-oscillation highlights the potential of memristor-based SNNs in applications such as image recognition.

Furthermore, a fully connected SNN based on our ZnO memristors was constructed for MNIST image classification, as depicted in Fig. 5a. The encoding function of oscillation neurons is simulated by the fitting curve in Fig. 4c, while the output neurons are described by an LIF neuron model. The threshold voltage and hold voltage are set based on the experimental data in Fig. 2a. The training progress contains a forward pass and a backward pass, while the testing progress only contains the forward pass.

In the forward pass, the ZnO oscillation neurons encode the input images into spike trains with different frequencies, and the input spikes are linearly transformed by the synaptic weights of a 784 × 10 fully connected layer. The output neurons integrate the postsynaptic currents in temporal and spatial domains, leak over time, and fire when their membrane potential reaches the threshold voltage. The index of the output neuron with the highest firing rate corresponds to the predicted result.

In the backward pass, the mean square error (MSE) is used as the loss function to measure the error between the target labels and predicted labels. The back-propagation through time (BPTT) is applied to train the weights of the fully connected layer. To avoid using a non-differentiable step activation function of spiking neurons, a sigmoid function is used as the surrogate function for gradient calculations.

Here, a total of 60,000 images were used for training, while 10,000 images were used for testing. The SNN model was constructed and trained using SpikingJelly. Fig. 5b demonstrates the accuracy in the test dataset, which reaches 89.17% after 50 epochs. Fig. 5c shows the average spiking counts of output neurons after training, with columns representing target labels and rows indicating neuron indexes. The output neuron corresponding to the target label has a high firing rate, while other neurons fire at a very low rate, resulting in high energy efficiency. The confusion matrix of the classification result is illustrated as Fig. 5d, demonstrating that most images are correctly identified by the SNN based on our ZnO memristors.

CONCLUSIONS

Artificial neurons are essential components of neuromorphic computing, enabling SNNs to efficiently replicate the low-power processes of the biological brain. This study highlights the promising potential of Pt/Ag/ZnO/Pt-based diffusive memristors for such applications. These memristors demonstrate excellent volatile threshold-switching characteristics, rapid

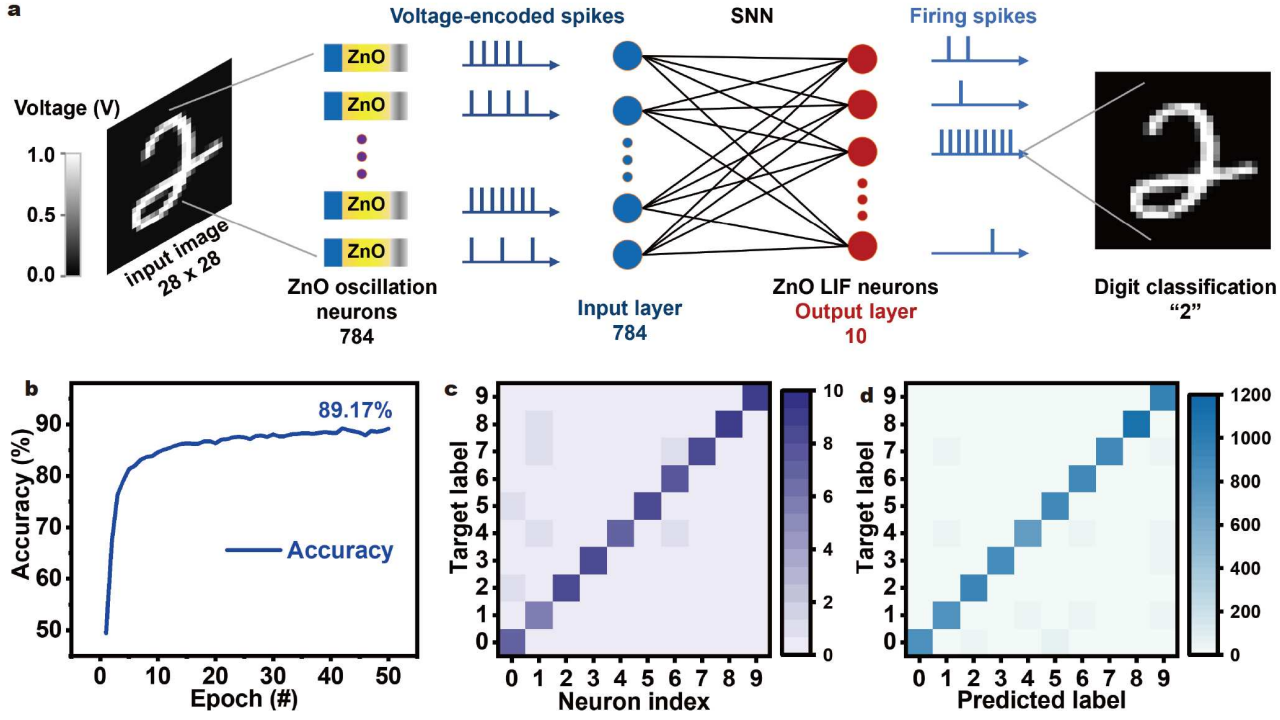

Figure 5 The simulation of an SNN based on Pt/Ag/ZnO/Pt LIF memristors for MNIST image classification. (a) Schematic diagram of a trained SNN for the MNIST image classification. (b) Image classification accuracy with 50 training epochs. (c) The average spike counts of output neurons with different input images. (d) Confusion matrix of classification results after training.

response times, and high endurance, making them well-suited to effectively emulate both LIF and oscillatory neurons. By integrating these memristors into an SNN, we achieved a classification accuracy of 89.17% on the MNIST dataset, showcasing their capability to efficiently handle complex computational tasks. These findings position ZnO diffusive memristors as promising artificial neurons for the development of energy-efficient and high-performance neuromorphic systems, bringing us closer to bridging the gap between artificial and biological neural processing.

Received 27 November 2024; accepted 30 December 2024; published online 24 January 2025

1 Shi T, Wang R, Wu Z, *et al.* A review of resistive switching devices: performance improvement, characterization, and applications. Small Struct, 2021, 2: 2000109
2 Yang Y, Zhu F, Zhang X, *et al.* Firing feature-driven neural circuits with scalable memristive neurons for robotic obstacle avoidance. Nat Commun, 2024, 15: 4318
3 John RA, Demirağ Y, Shynkarenko Y, *et al.* Reconfigurable halide perovskite nanocrystal memristors for neuromorphic computing. Nat Commun, 2022, 13: 2074
4 Duan Q, Jing Z, Zou X, *et al.* Spiking neurons with spatiotemporal dynamics and gain modulation for monolithically integrated memristive neural networks. Nat Commun, 2020, 11: 3399
5 Sarkar T, Lieberth K, Pavlou A, *et al.* An organic artificial spiking neuron for *in situ* neuromorphic sensing and biointerfacing. Nat Electron, 2022, 5: 774–783
6 Yang K, Joshua Yang J, Huang R, *et al.* Nonlinearity in memristors for neuromorphic dynamic systems. Small Sci, 2022, 2: 2100049
7 Huang HM, Yang R, Tan ZH, *et al.* Quasi-hodgkin-huxley neurons with leaky integrate-and-fire functions physically realized with memristive devices. Adv Mater, 2019, 31: 1803849
8 Stoliar P, Tranchant J, Corraze B, *et al.* A leaky-integrate-and-fire neuron analog realized with a Mott insulator. Adv Funct Mater, 2017, 27: 1604740
9 Liu H, Qin Y, Chen HY, *et al.* Artificial neuronal devices based on emerging materials: neuronal dynamics and applications. Adv Mater, 2023, 35: 2205047
10 Fu T, Liu X, Gao H, *et al.* Bioinspired bio-voltage memristors. Nat Commun, 2020, 11: 1861
11 Duan Q, Zhang T, Liu C, *et al.* Artificial multisensory neurons with fused haptic and temperature perception for multimodal in-sensor computing. Adv Intelligent Syst, 2022, 4: 2200039
12 Li X, Zhong Y, Chen H, *et al.* A memristors-based dendritic neuron for high-efficiency spatial-temporal information processing. Adv Mater, 2023, 35: 2203684
13 Kumar S, Strachan JP, Williams RS. Chaotic dynamics in nanoscale NbO_2 Mott memristors for analogue computing. Nature, 2017, 548: 318–321
14 Noé P, Verdy A, d'Acapito F, *et al.* Toward ultimate nonvolatile resistive memories: the mechanism behind ovonic threshold switching revealed. Sci Adv, 2020, 6: eaay2830
15 Yuan Z, Li X, Song S, *et al.* The enhanced performance of a Si–As–Se ovonic threshold switching selector. J Mater Chem C, 2021, 9: 13376–13383
16 Lee H, Cho SW, Kim SJ, *et al.* Three-terminal ovonic threshold switch (3T-OTS) with tunable threshold voltage for versatile artificial sensory neurons. Nano Lett, 2022, 22: 733–739
17 Zhao X, Ma J, Xiao X, *et al.* Breaking the current-retention dilemma in cation-based resistive switching devices utilizing graphene with controlled defects. Adv Mater, 2018, 30: 1705193
18 Chen S, Zhang T, Tappertzhofen S, *et al.* Electrochemical-memristor-based artificial neurons and synapses—fundamentals, applications, and challenges. Adv Mater, 2023, 35: 2301924
19 Zhang X, Wang W, Liu Q, *et al.* An artificial neuron based on a threshold switching memristor. IEEE Electron Device Lett, 2018, 39: 308–311
20 Wang Z, Rao M, Midya R, *et al.* Threshold switching of Ag or Cu in dielectrics: materials, mechanism, and applications. Adv Funct Mater, 2018, 28: 1704862
21 Hua Q, Wu H, Gao B, *et al.* A threshold switching selector based on highly ordered Ag nanodots for X-point memory applications. Adv Sci, 2019, 6: 1900024
22 Ma Z, Chen W, Cao X, *et al.* Criticality and neuromorphic sensing in a single memristor. Nano Lett, 2023, 23: 5902–5910
23 Jhang WC, Hsu CC. Coexistence of nonvolatile WORM, bipolar, unipolar, and volatile resistive switching characteristics in a dry oxide layer with Ag conductive bridges. IEEE Trans Electron Devices, 2022, 69: 4914–4919
24 Chekol SA, Menzel S, Ahmad RW, *et al.* Effect of the threshold kinetics on the filament relaxation behavior of Ag-based diffusive memristors. Adv Funct Mater, 2022, 32: 2111242
25 Dou H, Lin Z, Hu Z, *et al.* Self-assembled Au nanoelectrodes: enabling low-threshold-voltage HfO_2-based artificial neurons. Nano Lett, 2023, 23: 9711–9718
26 Chen C, He Y, Mao H, *et al.* A photoelectric spiking neuron for visual depth perception. Adv Mater, 2022, 34: 2201895
27 Kim J, Choi JH, Kim S, *et al.* Transition of short-term to long-term memory of Cu/TaO_x/CNT conductive bridge random access memory for neuromorphic engineering. Carbon, 2023, 215: 118438
28 Liu Y, Wang H, Lin J, *et al.* Stretchable and stable neuromorphic tactile system. J Mater Chem C, 2024, 12: 10979–10984
29 Zeng YH, Chu FJ, Shih LC, *et al.* Dual light temporal coding modes enabled by nanoparticle-mediated phototransistors via gate bias modulation for brain-inspired visual perception. ACS Appl Mater Interfaces, 2023, 15: 9563–9573
30 Chen J, Liu X, Liu C, *et al.* Reconfigurable Ag/HfO_2/NiO/Pt memristors with stable synchronous synaptic and neuronal functions for renewable homogeneous neuromorphic computing system. Nano Lett, 2024, 24: 5371–5378
31 Shi K, Heng S, Wang X, *et al.* An oxide based spiking thermoreceptor for low-power thermography edge detection. IEEE Electron Device Lett, 2022, 43: 2196–2199
32 Cao Y, Wang S, Wang R, *et al.* Physically transient artificial neuron based on Mg/magnesium oxide threshold switching memristor. IEEE Trans Electron Devices, 2023, 70: 2047–2051
33 Wang Z, Joshi S, Savel'ev S, *et al.* Fully memristive neural networks for pattern classification with unsupervised learning. Nat Electron, 2018, 1: 137–145
34 Hua Q, Wu H, Gao B, *et al.* Low-voltage oscillatory neurons for memristor-based neuromorphic systems. Glob Challenges, 2019, 3: 1900015
35 Li Y, Tang J, Gao B, *et al.* Oscillation neuron based on a low-variability threshold switching device for high-performance neuromorphic computing. J Semicond, 2021, 42: 064101
36 Russo P, Xiao M, Liang R, *et al.* UV-induced multilevel current amplification memory effect in zinc oxide rods resistive switching devices. Adv Funct Mater, 2018, 28: 1706230
37 Jiang J, Xiao W, Li X, *et al.* Hardware-level image recognition system based on ZnO photo-synapse array with the self-denoising function. Adv Funct Mater, 2024, 34: 2313507
38 Xu L, Wang W, Li Y, *et al.* N:ZnO/MoS_2-heterostructured flexible synaptic devices enabling optoelectronic co-modulation for robust artificial visual systems. Nano Res, 2024, 17: 1902–1912
39 Qileng A, Liu W, Sun Z, *et al.* Portable dual-modular immunosensor constructed from bimetallic metal-organic framework heterostructure grafted with enzyme-mimicking label for rosiglitazone detection. Adv Funct Mater, 2022, 32: 2203244
40 Pham PQ, Duong TBN, Le NQN, *et al.* Synaptic behavior in analog memristors based on green-synthesized ZnO nanoparticles. Ceramics Int, 2024, 50: 28480–28489
41 Ranjbari A, Demeestere K, Kim KH, *et al.* Oxygen vacancy modification of commercial ZnO by hydrogen reduction for the removal of thiabendazole: characterization and kinetic study. Appl Catal B-Environ,

2023, 324: 122265
42 Dang B, Liu K, Wu X, *et al.* One-phototransistor-one-memristor array with high-linearity light-tunable weight for optic neuromorphic computing. Adv Mater, 2023, 35: 2204844
43 Yuan R, Duan Q, Tiw PJ, *et al.* A calibratable sensory neuron based on epitaxial VO_2 for spike-based neuromorphic multisensory system. Nat Commun, 2022, 13: 3973
44 Choi W, Kwon O, Lee J, *et al.* Volatile threshold switching devices for hardware security primitives: exploiting intrinsic variability as an entropy source. Appl Phys Rev, 2024, 11: 021323
45 Jiang Y, Wang D, Lin N, *et al.* Spontaneous threshold lowering neuron using second-order diffusive memristor for self-adaptive spatial attention. Adv Sci, 2023, 10: 2301323
46 Lu YF, Li Y, Li H, *et al.* Low-power artificial neurons based on Ag/TiN/$HfAlO_x$/Pt threshold switching memristor for neuromorphic computing. IEEE Electron Device Lett, 2020, 41: 1245–1248
47 Yang JH, Mao SC, Chen KT, *et al.* Emulating nociceptive receptor and LIF neuron behavior via ZrO_x-based threshold switching memristor. Adv Elect Mater, 2023, 9: 2201006
48 Peng W, Liu C, Xu C, *et al.* Fully printed IGZO memristor arrays with robust threshold switching characteristics for artificial nociceptors. Sci China Mater, 2024, 67: 2661–2670
49 Song YG, Kim JE, Kwon JU, *et al.* Highly reliable threshold switching characteristics of surface-modulated diffusive memristors immune to atmospheric changes. ACS Appl Mater Interfaces, 2023, 15: 5495–5503
50 Jo Y, Woo DY, Noh G, *et al.* Hardware implementation of network connectivity relationships using 2D hBN-based artificial neuron and synaptic devices. Adv Funct Mater, 2024, 34: 2309058
51 Han JK, Yun SY, Lee SW, *et al.* A review of artificial spiking neuron devices for neural processing and sensing. Adv Funct Mater, 2022, 32: 2204102
52 Hong Y, Liu Y, Li R, *et al.* Emerging functions of two-dimensional materials in memristive neurons. J Phys Mater, 2024, 7: 032001
53 Zuo W, Zhu Q, Fu Y, *et al.* Volatile threshold switching memristor: an emerging enabler in the AIoT era. J Semicond, 2023, 44: 053102

Acknowledgement This work was supported by the National Natural Science Foundation of China (62471190) and the Natural Science Foundation of Hubei Province, China (2022CFA031).

Author contributions Wang L conceived and directed this research, performed the experiments, analyzed the date, and wrote the manuscript. Zhang L contributed to the circuit design and simulation. Hua S contributed to the experimental improvements. Guo X and Fu Q provided support for the advancement of the project.

Conflict of interest The authors declare that they have no conflict of interest.

Liang Wang received his Bachelor of Engineering (BE) and Master of Arts (MA) degrees from China University of Mining and Technology and Huazhong University of Science and Technology (HUST), respectively. He is currently a PhD student at the School of Integrated Circuits, HUST. His current research interest is neuromorphic electronic devices and systems.

Qiuyun Fu is a professor at the School of Integrated Circuits, HUST, Wuhan, China. She received her PhD degree in materials science from TU Dresden in 2005. She served as a scientist at Fraunhofer IPMS, Germany. Her current research focuses on information storage devices, thin film devices, chip-scale integrated components and chip-scale integrated components.

Xin Guo is a distinguished professor at the School of Materials Science and Engineering, HUST, Wuhan, China. Before joining HUST in 2012, from 2002 to 2012, he was a senior scientist at the Research Center Juelich, Germany; from 1998 to 2002, he was working at the Max Planck Institute for Solid State Research, Stuttgart, Germany. In 2005, he received the Ross Coffin Purdy Award from the American Ceramic Society. His current research focuses on neuromorphic devices, systems and artificial intelligence; gas sensors and artificial intelligent sensing; solid electrolytes and solid-state batteries.

基于ZnO扩散型忆阻器的漏电整合发放神经元和振荡神经元用于脉冲神经网络

汪亮[1,2], 张乐[2], 化帅斌[2], 傅邱云[1*], 郭新[2*]

摘要 扩散型阈值转变忆阻器已成为人工神经元的有前景候选者，能够有效模拟神经元功能，并通过脉冲神经网络模拟生物大脑的低功耗处理. 在本研究中，我们提出了一种基于Pt/Ag/ZnO/Pt扩散型忆阻器的人工神经元，该忆阻器展现出优异的阈值开关特性，包括不需要电预处理、低电压工作(<0.2 V)、高稳定性(在1024个循环中的变化系数仅为2.25%)、高开关比(10^6)以及固有的自适应特性. 这些Pt/Ag/ZnO/Pt扩散型忆阻器被用于同时模拟振荡神经元和泄漏积分发放(LIF)神经元，通过改变脉冲参数精确调节振荡和发放频率，同时保持低能耗(每个脉冲1.442 nJ). 我们进一步将振荡神经元和LIF神经元分别集成作为输入和输出神经元，构建了一个两层的脉冲神经网络，在基于MNIST的电压图像上实现了89.17%的高分类准确率. 这项工作强调了ZnO扩散型忆阻器在模拟人工神经元方面的潜力，并突显了它们在使用脉冲神经网络进行先进类脑计算应用中的前景.